Journal of Materials Chemistry

Cite this: *J. Mater. Chem.*, 2011, **21**, 14150

www.rsc.org/materials

FEATURE ARTICLE

Principles of voxel refinement in optical direct write lithography†

Timothy F. Scott,[a] Christopher J. Kloxin,[b] Darren L. Forman,[c] Robert R. McLeod[c] and Christopher N. Bowman*[a]

Received 2nd May 2011, Accepted 16th June 2011
DOI: 10.1039/c1jm11915j

Optical direct write lithography (ODWL) has the capacity for generating three dimensional arbitrary patterns. Here we examine principles for voxel refinement and relate several techniques for achieving nanoscale resolution. The influence of optics, gelation, and polymerization scaling behavior are expounded, demonstrating the necessity for adopting a multidisciplinary mindset to control both voxel dimensions and minimize out-of-focus reactions. Aspects of two-photon ODWL are reviewed and recent multi-beam ODWL approaches that draw inspiration from STED microscopy are examined.

1. Introduction

Several maskless lithographic approaches, including nanoimprint lithography, dip pen lithography, electron beam & focused ion beam lithography, scanning near-field lithography, and optical direct write lithography (ODWL), have emerged that are capable of fabricating arbitrary, non-periodic patterns with feature sizes on the order of tens to hundreds of nanometres. These approaches are typically utilized to create relief patterns on a surface; however, ODWL is additionally capable of fabricating three-dimensional nanostructures *via* the scanning of a 'writing stylus', consisting of the focal point of a focused laser beam, through a photoresist volume.

The advent of ODWL has enabled the fabrication of a vast array of three-dimensional objects with applications ranging from photonic metamaterials[1–4] to cell culture scaffolds[5–7] to mechanical microdevices.[8–12] Structures fabricated by ODWL are comprised of voxels, the smallest volume elements of material that a lithographic system is capable of fabricating, and advances in the ODWL field have led to impressive refinements in voxel resolution. At the lowest resolution, conventional stereolithography, a rapid prototyping technique where parts are constructed in slices, typically yields multi-micrometre feature sizes[13] whereas single-photon, continuous wave ODWL is capable of yielding feature dimensions of several hundred nanometres.[8,11,14] Two-photon, pulsed ODWL approaches significantly improve the resolution and enable the fabrication of ~100 nm feature sizes.[3,9,10,15] More recently, ODWL schemes comprising multiple irradiation beams have further improved polymerization confinement, yielding feature sizes down to 10s of nanometres.[16–20] While dramatically improving the possible device complexity and value, these advances in voxel refinement require the incorporation of concurrent and complementary developments in both materials chemistry and optical physics. Herein, we examine select aspects of ODWL voxel refinement and illustrate the necessity of adopting a multidisciplinary development approach to this topic.

2. Nuts and bolts: the optics of ODWL

The voxel size produced by an ODWL system is primarily determined by the optical spot size at the focus of the writing beam; however, this spot size is fundamentally limited by diffraction and is described by the relations[21]

$$CD = \frac{k_1 \lambda}{NA},$$

and

$$DOF = \frac{k_2 \lambda}{NA^2}$$

where CD is the critical or smallest transverse dimension, DOF is the depth of focus or lateral dimension, k_1 and k_2 are engineering parameters on the order of unity, λ is the wavelength, and NA is the numerical aperture. The NA refers to the extent of the cone of light transmitted by a lens and is defined as[21]

$$NA = n \sin(\theta),$$

where n is the ambient refractive index (1 for an air lens, ~1.52 for the oil used with an immersion lens) and θ is the angle between the edge of the light cone and the optical axis. The parameter k_1, as used in the photolithography literature, describes the cumulative effect of proximity effects, polarization and other factors that influence resolution.

[a]*Department of Chemical and Biological Engineering, University of Colorado, Boulder, CO, 80309-0424, USA. E-mail: christopher.bowman@colorado.edu*
[b]*Department of Materials Science and Engineering, and Department of Chemical Engineering, University of Delaware, Newark, Delaware, 19716, USA*
[c]*Department of Electrical, Computer, and Energy Engineering, University of Colorado, Boulder, Colorado, 80309-0425, USA*

† Electronic supplementary information (ESI) available. See DOI: 10.1039/c1jm11915j.

The *CD* and *DOF* produced by an ODWL system are highly dependent upon the components used in the system. The basic components of such a system include the light source, focusing optics, motion control and the photosensitive target material (Fig. 1). Lasers are ideal light sources owing to their high brightness, inherently narrow spectrum and good stability. Shorter irradiation wavelengths yield smaller dimensions, and thus, ODWL systems often use blue or UV laser emission wavelengths to improve resolution. Conditioning of the beam generated by the laser for the highest quality is essential to optimize the resolution. Beam conditioning is typically performed by employing an inline spatial filter to yield a beam approaching an ideal plane wave; as the beam increasingly departs from this phase-flat ideal, the aberrations increase and the system resolution is reduced. Here, the optical quality of an imaging system is described by the Strehl ratio which is the ratio of the observed peak intensity at the detection plane from a point source to the theoretical maximum peak intensity of a perfect imaging system working at the diffraction limit, where a value of unity signifies diffraction limited performance. This ratio is related to the root mean square wavefront error (*i.e.*, phase error), which may be measured with a Shack-Hartman or other wavefront sensor.

Transverse spot scanning is accomplished either through motion of the fabricated part or deflection of the writing beam. In the former case, precise linear motorized stages translate the part under a fixed lens focus. This approach allows large transverse part dimensions limited only by the stage travel; however, it is limited by slow translation speeds. Alternatively, the beam may be scanned across a stationary target. Mirrors attached to fast galvanometers can rapidly deflect the beam, causing a focused spot to be scanned across the target. This approach features high translation speeds; however, transverse dimensions are limited to the lens field of view, typically ~200 μm for high power objectives. Some commercial tools use both approaches to maximize both part size and writing speed.

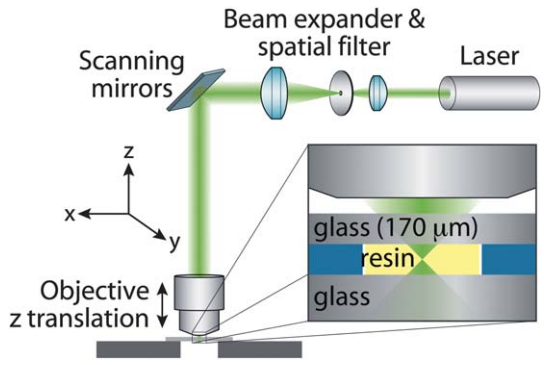

Fig. 1 Illustration of a scanning ODWL system. A laser beam, conditioned by a spatial filter, is deflected by mirrors attached to galvanometers which are imaged to the back focal plane of the objective (lenses not shown for clarity). Direct or external modulation of the laser, in combination with the scan mirrors, modifies the photosensitive material at a set of voxels in a transverse plane. Three-dimensional patterning is enabled by translating the focused spot in *z via* motorized objective or material translation.

Although the total transverse scale is set by the choice of scan hardware, total depth range is determined by the objective lens aberration limits and working distance. Microscope objective lenses are excellent choices as the focusing optical elements in ODWL systems as their high *NA* and optical aberration corrections enable the smallest focused spot diameters possible at a given wavelength. However, they are designed for a particular gap and cover slip thickness and aberrations, primarily spherical aberration, occur as the lens is moved to write in depth. High-power air objectives designed for 170 μm glass cover slips can suffer a two-fold resolution degradation if the cover slip thickness is reduced to 160 μm, motivating "high performance" cover slips with ±5 μm tolerance. Variation of the lens to cover slip gap with an air-immersion objective is similarly limited, severely restricting total part height. One solution is to use an immersion lens in which the gap is filled with oil whose refractive index is matched to the glass and the polymer. Note that the refractive index of water is not well matched and thus should be avoided. Index-matching removes aberration considerations as the refractive index along the axis now does not depend on lens height. In this case, only the lens working distance, measured from the last element to the focal plane, limits the total part height. Subtracting the cover slip thickness, this approach usually enables several hundred μm fabrication depth.

3. Liquid to solid: voxel refinement *via* gelation control

The chemistry of the photoresist is a critical factor affecting both the ultimate resolution achievable and the capacity for writing confinement by an ODWL system. Photopolymerizable resins, where the resin volume exposed to light polymerizes to form a crosslinked, insoluble gel, are commonly utilized in ODWL as negative tone photoresists. These polymerizations are typically mediated by either radicals or cations; the mechanism by which the polymerization proceeds is dependent upon the photoinitiator and polymerizable functionalities used. During the photopolymerization of a resin consisting of a multifunctional monomer, the molecular weight progressively increases until the gel point is reached, whereupon the molecular weight diverges. This gelled material is insoluble; thus, the gel point is a well-defined threshold for voxel fabrication as the gelled, insoluble material survives post-polymerization development whereas the bulk of the resin remains unpolymerized and soluble, enabling facile removal during development.

The gelation threshold can be utilized to fabricate voxels with transverse dimensions smaller than the diffraction limit by carefully limiting the degree of polymerization within the focused spot such that only the fraction of material under the highest irradiation intensity polymerizes beyond the gelation threshold (see Fig. 2). Several techniques have been utilized to limit this polymerization degree, either by simply reducing the irradiation intensity and duration, or by increasing the irradiation dose required to gel the material.[22] For example, by varying the exposure duration and laser pulse energy in the two-photon ODWL of an acrylate resin, transverse resolutions down to 120 nm were achieved.[9,10] Conversely, Park *et al.*[15] incorporated a radical polymerization inhibitor in their radically polymerizable photoresist, thus increasing the radical concentration

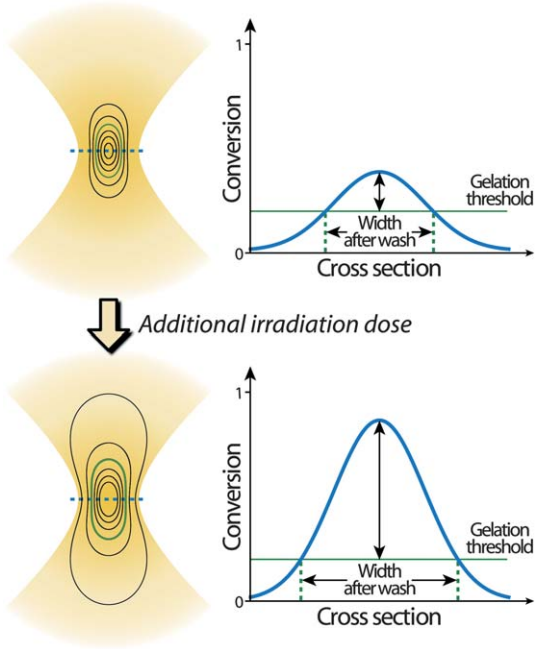

Fig. 2 Effect of reaction extent on gelled volume. The light intensity distribution of the focused beam yields a conversion gradient that is represented by contours (left), where the green contour represents the conversion at gelation. As the reaction proceeds (bottom left), more of the material is above the gelation threshold (right). Thus, by limiting the extent of reaction, a smaller volume of material remains after the solvent wash.

required for gelation, and attained a transverse resolution of ~100 nm. Unfortunately, these approaches necessarily reduce the contrast between the conversion of the gelled, insoluble material and the ungelled, soluble material; thus, the fabricated voxels are often loosely crosslinked, mechanically unsound structures unable to withstand the rigors of post-patterning solvent processing that are necessary for device fabrication.[15]

4. Mechanisms matter: polymerization scaling

The influence of the initiation rate on the reaction rate is an oft-overlooked consideration in ODWL systems. Focused laser light allows for the localization of photopolymerization to the vicinity of the focal point. While photopolymerization does occur in the out of focus regions, the single-photon absorption initiation rate (R_i) far from the focus approximately scales as $1/z^2$, where z is the distance from the focal point along the optical axis; one would expect that the polymerization rate would similarly decrease as a function of the inverse squared distance. However, owing to the well-known "steady-state approximation",[23] where the radical initiation rate is approximately equal to the radical termination rate,[23] the photopolymerization rate scales as $R_p \sim [R_i]^\alpha$, where α is between 0 and 1 and depends primarily on the termination mechanism. Thus, the spatial polymerization rate scaling exhibits a dependence on the distance, $R_p \sim z^{-2\alpha}$. Classical bimolecular termination exhibited by conventional free radical polymerizations yields α equal to $^1/_2$.[24] Deviations from the square-root dependence on R_i have been observed. For example, the capability of lasers to generate high intensities can readily promote primary radical termination, where the high concentration of initiating radicals leads to termination rather than propagation, resulting in $\alpha \to 0$ where the polymerization becomes completely unconfined. In contrast, there are several polymerizations, such as cationic[25] or radical-mediated thiol-ene[26] polymerizations, that exhibit $\alpha \to 1$ polymerization kinetics, which is typically attributed to unimolecular termination.

The scaling exponent α influences the material voxel size, the dimensions of which are characterized by

$$D_{FWHM} = \frac{2}{\pi}\frac{\lambda}{NA}\sqrt{\frac{\ln 2}{2m\alpha}} \quad (1)$$

and

$$L_{FWHM} = \frac{2n}{\pi}\frac{\lambda}{NA^2}\sqrt{2^{1/m\alpha} - 1}, \quad (2)$$

where D_{FWHM} and L_{FWHM} are the full width at half maximum voxel diameter (*i.e.*, transverse dimension) and length (axial dimension), respectively, and m is the photon absorption order (*e.g.*, $m = 1$ or 2 for single- or two-photon absorption, respectively). Specifically, eqn (1) and (2) describe the full width at half maximum extents of the transverse and axial steady-state excited photoinitiator concentrations created by a Gaussian intensity distribution (see ESI†). While two-photon absorption is proportional to the intensity squared ($m = 2$), the radical kinetics discussed above reduce the effective nonlinearity to the product of m and α. If we consider two polymerizable photoresists, one of which terminates by a classical bimolecular mechanism and the other by a unimolecular mechanism, we find that, under equivalent single-photon irradiation conditions, the voxel diameter and length ratios become

$$\frac{D_{FWHM}|_{\alpha=1}}{D_{FWHM}|_{\alpha=1/2}} = \frac{1}{\sqrt{2}} \quad \text{and} \quad \frac{L_{FWHM}|_{\alpha=1}}{L_{FWHM}|_{\alpha=1/2}} = \frac{1}{\sqrt{3}}. \quad (3)$$

Thus, a material exhibiting a scaling exponent of $\alpha = 1$ yields a 71% smaller voxel than an $\alpha = ^1/_2$ material.

An overarching concern associated with ODWL is the suppression of reaction in the out-of-focus regions of the writing beam. Although isolated voxel fabrication is ideally confined to the focal plane, the superposition of the many out-of-focus regions of densely-spaced voxels leads to undesired and unconfined reaction. For example, one may attempt to fabricate a wire perpendicular to the writing beam in a photoreactive material; however, the accumulated out-of-focus irradiation over the distance traveled to write the wire effects confinement loss (see Fig. 3). Increasing the product of m and α (see eqn (1) and (2)) dramatically reduces reaction in the out-of-focus regions, improving confinement.

5. Decreasing the odds: multi-photon absorption

Two-photon ODWL has been utilized by a number of researchers to realize the fabrication of 3D nanostructures.[1–3,9,10,15] The premise of these studies is that the confinement provided by localized, two-photon absorption (*i.e.*, $m = 2$) results in reaction only near the focus. Two-photon absorption requires the simultaneous absorption of two photons (see Fig. 4); thus, the absorption cross-section is very small. That

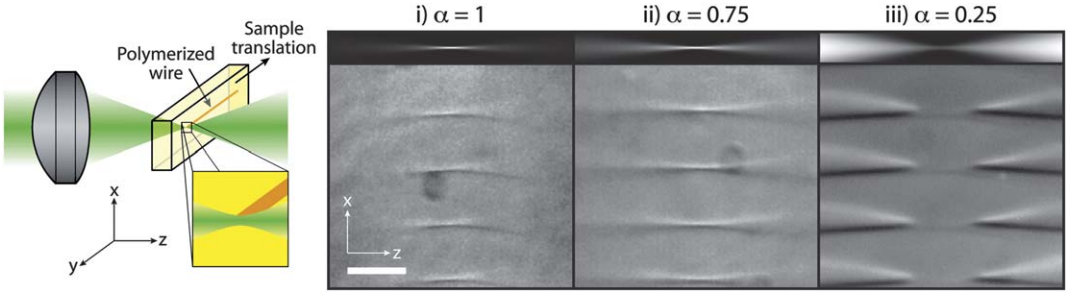

Fig. 3 Differential interference contrast micrographs of wires fabricated *via* single-photon ODWL. The refractive index structures shown were produced by irradiating holographic media (consisting of unreacted monomer embedded in a gelled matrix) with a single-photon, continuous wave focused laser beam translated along the y axis (see schematic) and microtomed in the xz plane.[27] The polymerization mechanisms include i) cationic, ii) radical, and iii) high irradiation intensity radical polymerizations. A decrease in the scaling exponent (α) effects a progressive loss of axial polymerization confinement. Scale bar, 35 μm.

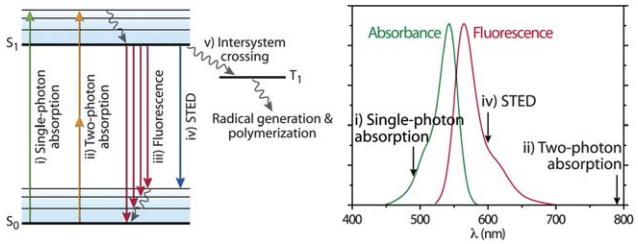

Fig. 4 A Jablonski diagram (left) and typical fluorophore absorbance and fluorescence spectra (right). Jablonski diagrams are schematic representations of molecular electronic transitions. (i) Upon irradiation, a molecule initially at its ground state (S_0, where S is a singlet) may absorb a photon of appropriate energy and transition to an excited state (S_1). (ii) At very high irradiation intensities, the molecule may absorb two photons of lower energy (*i.e.*, longer wavelength) simultaneously; if the sum of the energies is adequate, the molecule may transition to the excited state S_1. (iii) Fluorescence, a spontaneous emission mode, may occur as the molecule transitions back from S_1 to S_0 upon the emission of a photon. (iv) Irradiation of a molecule in its excited state at a wavelength resonant with the fluorescence emission, but sufficiently red-shifted to preclude ground state absorbance, can stimulate emission and deplete the excited state. (v) Molecules in their excited singlet state may undergo intersystem crossing to the excited triplet state (T_1); photoinitiators in the T_1 state may then generate radicals and initiate a polymerization.

two-photon absorption cross-sections (δ) are typically expressed in Goeppert–Mayer (GM) units, where 1 GM is 10^{-50} cm^4 s/photon, is indicative of the cross-section minuteness. Commercial photoinitiators typically exhibit δ values of less than 30 GM.[28] Owing to these small δ values, both high power sources such as ultrashort pulse Ti:sapphire lasers and slow translation rates are typically utilized in two-photon ODWL. Tremendous progress has been made in the design of chromophores with enhanced δ values. In particular, Marder and Perry developed chromophores consisting of donor (D) or acceptor (A) groups linked by a π-conjugate bridge (*i.e.*, D–π–D, D–π–A–π–D, and A–π–D–π–A) that exhibit extraordinarily large δ values, in excess of 10^3 GM, and demonstrated their utility in two-photon ODWL.[1,29] Semiconductor quantum dots have been developed that also exhibit large δ values, *i.e.*, greater than 10^4 GM,[30] and have been utilized as two-photon polymerization sensitizers.[31] As both organic and inorganic large δ chromophores typically exhibit low polymerization initiation quantum efficiencies,[31,32] significant room for efficiency improvements in the development of two-photon photoinitiation systems remains.

The extremely high irradiation intensities utilized in two-photon ODWL necessitate an absence of single-photon absorption in the photoresist to prevent charring of the material; thus, two-photon ODWL is typically performed by irradiation in the red to near infrared spectrum (~680–850 nm). Nevertheless, damage to the material may still occur at high irradiation doses.[33] Although two-photon absorption enables the facile fabrication of sub-diffraction feature sizes, the long writing wavelength results in surprisingly large feature sizes. The voxel fabricated by a two-photon process (*i.e.*, $m = 2$) would have a $2^1/_2$ and $3^1/_2$ times smaller D_{FWHM} and L_{FWHM}, respectively, than a voxel fabricated under equivalent single-photon irradiation conditions in an $\alpha = 1$ material. However, single-photon ODWL is still capable of yielding smaller voxels owing to its utilization of much shorter wavelengths. For example, single-photon irradiation at wavelengths shorter than 515 nm would yield smaller voxels than two-photon irradiation at 780 nm (commonly utilized in two-photon ODWL[34]). Shorter two-photon irradiation wavelengths, in conjunction with appropriately formulated photoresists, enable the fabrication of correspondingly smaller voxels. Recently, a two-photon irradiation wavelength of 520 nm was utilized to fabricate 65 nm feature sizes[3] by carefully limiting the extent of polymerization beyond gelation.

6. The next generation: multi-beam ODWL

In recent years, several ODWL schemes utilizing multiple superimposed irradiation beams have emerged that are capable of fabricating features sizes smaller than are commonly achievable *via* conventional single- or two-photon ODWL approaches and well below the diffraction limit. Each of these emergent lithography schemes originate from a superresolution optical microscopy technique developed by Stefan Hell and coworkers called Stimulated Emission Depletion (STED) microscopy.[35,36] The STED microscope is superficially similar to a conventional laser scanning confocal microscope in that a Gaussian excitation beam at λ_1 is projected into the sample under examination, exciting a fluorophore within the sample. However, in STED microscopy, an additional shaped beam with a dark center (*e.g.*, a 2D Gauss-Laguerre 'donut' mode or a 3D 'bottle-beam'[37]) at λ_2

is superimposed on the excited volume immediately subsequent to the first irradiation, stimulating the depletion of the excited state of the fluorophore (see Fig. 4) prior to fluorescence exclusively at the periphery of the excitation volume. Thus, the volume of the spheroid that fluoresces is very much refined relative to the original excited volume. Increasing the intensity of the STED beam increases the depletion at the excitation spot periphery and yields a concomitant resolution improvement (Fig. 5), theoretically without limit. Indeed, transverse resolutions below 10 nm have been achieved with STED microscopy.[38]

The STED mechanism should be equally applicable to radical-mediated ODWL, where, instead of depleting the excited state of a fluorophore, excited state depletion of a photoinitiator would occur prior to intersystem crossing from S_1 to T_1 and subsequent radical generation (Fig. 4). Efficient stimulated depletion of the excited state requires a large oscillator strength between S_0 and S_1[39] whereas, unfortunately, the oscillator strengths of Norrish type I (*i.e.*, photoscission) radical photoinitiators tend to be relatively small. Moreover, a small S_0–S_1 oscillator strength typically corresponds to large oscillator strengths between S_1 and higher excitation states.[19] As a result, absorption to higher singlet excitation states competes with stimulated emission from S_1. Since these higher excitation states tend to have faster intersystem crossing rates, the polymerization initiation rate can actually increase rather than decrease in the volume where depletion of the excited state is intended.[17,19] Despite this, the application of STED to a radical-mediated ODWL system was recently demonstrated utilizing a thioxanthone-based photoinitiator.[18] Here, two-photon irradiation at 810 nm was utilized to excite the photoinitiator whereas depletion of the photoinitiator excited state, prior to singlet to triplet intersystem crossing and radical generation, was accomplished by concurrent, continuous irradiation at 532 nm. Exposure of the material exclusively to the high power two-photon irradiation yielded polymerized structures; however, superposition of the second, depletion irradiation prevented polymerization from proceeding. A transverse resolution of 155 nm was achieved by exclusively two-photon irradiation; however, as the intensity of the superimposed depletion beam, manipulated into a donut-shaped mode, was increased, the excited state of the photoinitiator was progressively depleted at the periphery of the first Gaussian spot and the transverse resolution improved to 65 nm. Interestingly, a feature size minimum occurred as the intensity of the donut-shaped irradiation was increased, which was attributed to parasitic two-photon absorption of the depletion beam.

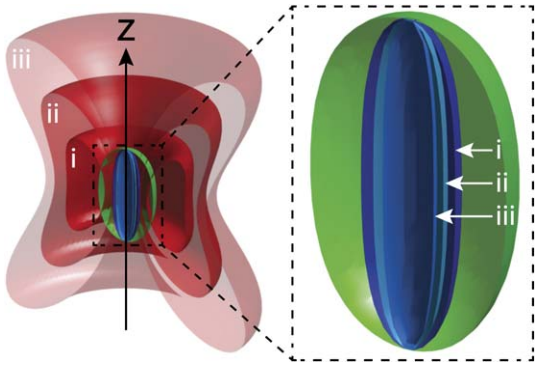

Fig. 5 Voxel refinement by excitation depletion. As the superimposed Gauss-Laguerre excitation depletion beam intensity is increased (red isosurfaces, i → iii), the transverse resolution (initial Gaussian intensity green isosurface) is progressively refined (blue isosurfaces, i → iii). Utilization of a bottle beam[37] (omitted for clarity) would effect a corresponding improvement in axial resolution.

The Fourkas group developed an alternative approach to achieving superresolution ODWL that also utilizes a multi-beam irradiation scheme but exploits a unique mechanism to deplete the photoinitiator excited state.[17] After exciting malachite green carbinol base to its S_1 excited state *via* two-photon absorption with an ultrafast, pulsed laser beam, depletion of the excited state was performed using a continuous wave laser beam of the same wavelength. By shaping the deactivation beam and superimposing it on the volume excited by the two-photon absorption, this approach, termed Resolution Augmentation through Photo-Induced Deactivation (RAPID) photolithography, yielded an axial resolution of 40 nm, which is an extraordinary improvement from the 600 nm resolution achieved in the absence of the continuous wave deactivation beam.

A third approach to refining voxel dimensions utilizing multiple irradiation beams was developed in our own labs. In a two-color irradiation scheme that is analogous to that utilized in STED microscopy, initiating species are generated by irradiation at λ_1; however, instead of depleting the excited state of the photoinitiator at the periphery of the excited volume, inhibiting species are generated by irradiation at λ_2.[16] Co-irradiation at λ_2 prematurely terminates the growing polymer chains, dramatically reducing the polymerization rate and delaying gelation of the material, thus enhancing spatial control of the polymerization. Importantly, success of this approach necessitates independent photocontrol over the two distinct photoactive species. This desired outcome is readily achieved by ensuring non-overlapping regions in the absorbance spectra of the photoinitiator and photoinhibitor. As the generation of the initiating and inhibiting radical species can be performed at modest irradiation intensities, this approach is economically very attractive as inexpensive, continuous wave diode lasers can be utilized as the two light sources. In the preliminary study of this approach where a 0.45 *NA* microscope objective was utilized, the transverse resolution varied dramatically as the inhibition irradiation intensity was increased, from 3.6 μm in the absence of λ_2 down to 200 nm at the highest λ_2 irradiation intensity.[16] Employment of a higher *NA* lens would yield further voxel refinement.

7. Conclusion

The refinement of ODWL voxel dimensions requires the consideration of several experimental factors. Minimization of the focused spot size is readily achieved *via* laser beam conditioning, utilizing high *NA* lenses, and refractive index matching. Beyond the elements of the optical train, the simplest approach to voxel refinement is to carefully control the reaction extent beyond the gel-point. This is accomplished straightforwardly by controlling irradiation dose. Alternatively, incorporation of compounds that consume or impede the polymerization active species increases in the irradiation dose required for gelation.

The reaction mechanism informs the mode by which polymerizations terminate, dictating the intensity scaling of the

polymerization rate. Polymerization mechanisms that yield high intensity scaling exponents are capable of fabricating finer voxel dimensions. The dependence upon intensity necessitates attention to both the spatial irradiation intensity gradient that is inherent in ODWL and the path over which the focused laser beam is scanned. In particular, axial confinement of the polymerization, when fabricating dense structures, is improved with higher intensity scaling exponents.

Two-photon ODWL has been used extensively owing to its capacity for improved voxel refinement and reduced reaction in the out-of-focus region. Although the two-photon absorption cross-sections of conventional photoinitiators are extraordinarily small, ongoing development has yielded new chemistries with enhanced cross-sections. Sophisticated ODWL techniques utilizing multiple irradiation beams have already demonstrated voxel fabrication resolutions matching that of two-photon approaches and are likely to achieve still further resolution refinements with the capacity for arbitrary patterning in three-dimensions on a nanoscopic scale.

Acknowledgements

The authors acknowledge funding from the National Science Foundation Grants CBET 0933828 and OII-0539731.

References

1 B. H. Cumpston, S. P. Ananthavel, S. Barlow, D. L. Dyer, J. E. Ehrlich, L. L. Erskine, A. A. Heikal, S. M. Kuebler, I. Y. S. Lee, D. McCord-Maughon, J. Q. Qin, H. Rockel, M. Rumi, X. L. Wu, S. R. Marder and J. W. Perry, *Nature*, 1999, **398**, 51–54.
2 J. Serbin, A. Egbert, A. Ostendorf, B. N. Chichkov, R. Houbertz, G. Domann, J. Schulz, C. Cronauer, L. Frohlich and M. Popall, *Opt. Lett.*, 2003, **28**, 301–303.
3 W. Haske, V. W. Chen, J. M. Hales, W. T. Dong, S. Barlow, S. R. Marder and J. W. Perry, *Opt. Express*, 2007, **15**, 3426–3436.
4 S. Shukla, E. P. Furlani, X. Vidal, M. T. Swihart and P. N. Prasad, *Adv. Mater.*, 2010, **22**, 3695–3699.
5 S. H. Lee, J. J. Moon and J. L. West, *Biomaterials*, 2008, **29**, 2962–2968.
6 T. Weiss, G. Hildebrand, R. Schade and K. Liefeith, *Eng. Life Sci.*, 2009, **9**, 384–390.
7 A. M. Kasko and D. Y. Wong, *Future Med. Chem.*, 2010, **2**, 1669–1680.
8 S. Maruo and K. Ikuta, *Appl. Phys. Lett.*, 2000, **76**, 2656–2658.
9 S. Kawata, H. B. Sun, T. Tanaka and K. Takada, *Nature*, 2001, **412**, 697–698.
10 T. Tanaka, H. B. Sun and S. Kawata, *Appl. Phys. Lett.*, 2002, **80**, 312–314.
11 S. Maruo and K. Ikuta, *Sens. Actuators, A*, 2002, **100**, 70–76.
12 G. Knoner, S. Parkin, T. A. Nieminen, V. L. Y. Loke, N. R. Heckenberg and H. Rubinsztein-Dunlop, *Opt. Express*, 2007, **15**, 5521–5530.
13 F. P. W. Melchels, J. Feijen and D. W. Grijpma, *Biomaterials*, 2010, **31**, 6121–6130.
14 M. Thiel, J. Fischer, G. von Freymann and M. Wegener, *Appl. Phys. Lett.*, 2010, **97**, 221102.
15 S. H. Park, T. W. Lim, D. Y. Yang, R. H. Kim and K. S. Lee, *Macromol. Res.*, 2006, **14**, 559–564.
16 T. F. Scott, B. A. Kowalski, A. C. Sullivan, C. N. Bowman and R. R. McLeod, *Science*, 2009, **324**, 913–917.
17 L. J. Li, R. R. Gattass, E. Gershgoren, H. Hwang and J. T. Fourkas, *Science*, 2009, **324**, 910–913.
18 J. Fischer, G. von Freymann and M. Wegener, *Adv. Mater.*, 2010, **22**, 3578–3582.
19 J. T. Fourkas, *J. Phys. Chem. Lett.*, 2010, **1**, 1221–1227.
20 M. P. Stocker, L. J. Li, R. R. Gattass and J. T. Fourkas, *Nat. Chem.*, 2011, **3**, 223–227.
21 W. M. Moreau, in *Semiconductor Lithography: Principles, Practices, and Materials*, Plenum Press, New York, 1988, pp. 364–365.
22 K. S. Lee, R. H. Kim, P. Prabhakaran, D. Y. Yang, T. W. Lim and S. H. Park, *J. Nonlinear Opt. Phys. Mater.*, 2007, **16**, 59–73.
23 P. J. Flory, in *Principles of Polymer Chemistry*, Cornell University Press, Ithaca, 1953, pp. 106–177.
24 H. B. Sun, T. Tanaka and S. Kawata, *Appl. Phys. Lett.*, 2002, **80**, 3673–3675.
25 S. H. Chen, W. D. Cook and F. Chen, *Macromolecules*, 2009, **42**, 5965–5975.
26 T. F. Scott, C. J. Kloxin, R. B. Draughon and C. N. Bowman, *Macromolecules*, 2008, **41**, 2987–2989.
27 A. C. Sullivan, M. W. Grabowski and R. R. McLeod, *Proc. SPIE–Int. Soc. Opt. Eng.*, 2006, **6335**, 63350F.
28 K. J. Schafer, J. M. Hales, M. Balu, K. D. Belfield, E. W. V. Stryland and D. J. Hagan, *J. Photochem. Photobiol., A*, 2004, **162**, 497–502.
29 M. Albota, D. Beljonne, J. L. Bredas, J. E. Ehrlich, J. Y. Fu, A. A. Heikal, S. E. Hess, T. Kogej, M. D. Levin, S. R. Marder, D. McCord-Maughon, J. W. Perry, H. Rockel, M. Rumi, C. Subramaniam, W. W. Webb, X. L. Wu and C. Xu, *Science*, 1998, **281**, 1653–1656.
30 D. R. Larson, W. R. Zipfel, R. M. Williams, S. W. Clark, M. P. Bruchez, F. W. Wise and W. W. Webb, *Science*, 2003, **300**, 1434–1436.
31 N. C. Strandwitz, A. Khan, S. W. Boettcher, A. A. Mikhailovsky, C. J. Hawker, T. Q. Nguyen and G. D. Stucky, *J. Am. Chem. Soc.*, 2008, **130**, 8280–8288.
32 S. R. Marder, J. L. Bredas and J. W. Perry, *MRS Bull.*, 2007, **32**, 561–565.
33 S. A. Pruzinsky and P. V. Braun, *Adv. Funct. Mater.*, 2005, **15**, 1995–2004.
34 S. H. Park, D. Y. Yang and K. S. Lee, *Laser Photonics Rev.*, 2009, **3**, 1–11.
35 S. W. Hell and J. Wichmann, *Opt. Lett.*, 1994, **19**, 780–782.
36 T. A. Klar, S. Jakobs, M. Dyba, A. Egner and S. W. Hell, *Proc. Natl. Acad. Sci. U. S. A.*, 2000, **97**, 8206–8210.
37 J. Arlt and M. J. Padgett, *Opt. Lett.*, 2000, **25**, 191–193.
38 E. Rittweger, K. Y. Han, S. E. Irvine, C. Eggeling and S. W. Hell, *Nat. Photonics*, 2009, **3**, 144–147.
39 K. Kolmakov, V. N. Belov, J. Bierwagen, C. Ringemann, V. Muller, C. Eggeling and S. W. Hell, *Chem.–Eur. J.*, 2010, **16**, 158–166.